Linear and Quasilinear Model for Pressure-Driven Interchange and Entropy Modes in a Warm Electron Dipole Plasma

Mike Mauel, Darren Garnier, Max Roberts, and Jay Kesner
Dept of Applied Physics and Applied Math, Columbia University, New York, NY USA
Plasma Science and Fusion Center, MIT, Cambridge, MA USA

56th Annual Meeting of the APS-Division of Plasma Physics
New Orleans, Louisiana
Poster GP8.0070 October 28, 2014

Abstract

The measured structures of electrostatic interchange modes in dipole-confined plasma cause global mixing when driven by energetic trapped electrons, sonic plasma, or warm electron pressure. Global circulation also appears in planetary magnetospheres driven by solar wind, but differences exist in underlying physics. Breaking azimuthal symmetry in magnetospheres caused currents to flow through the ionosphere, which regulate interchange motion [2]. In the laboratory, there are no field-aligned currents and perturbations induce ion-inertial currents, which determine the global linear model structure. In this poster, the linear description of global interchange and entropy modes are presented for the CTX and LDX laboratory magnetospheres computed from the flux-tube averaged gyrofluid equations [3]. Additionally, the quasilinear particle and heat flux are calculated and show turbulent self-organization that drives profiles to become centrally-peaked [4].

[1] NSF-DOE Plasma Sci Grants DE-FG02-00ER54585 and PHY-1201896.

[2] Lyon, *Science*, **288**, 1987 (2000).
[3] Ricci, *et al.*, *Phys Plasmas*, **13,** 062102 (2006).
[4] Kesner, *et al.*, *Phys Plasmas*, **18**, 050703 (2011).

Two Laboratory Magnetospheres: Plasma Experiments without Field-Aligned Currents

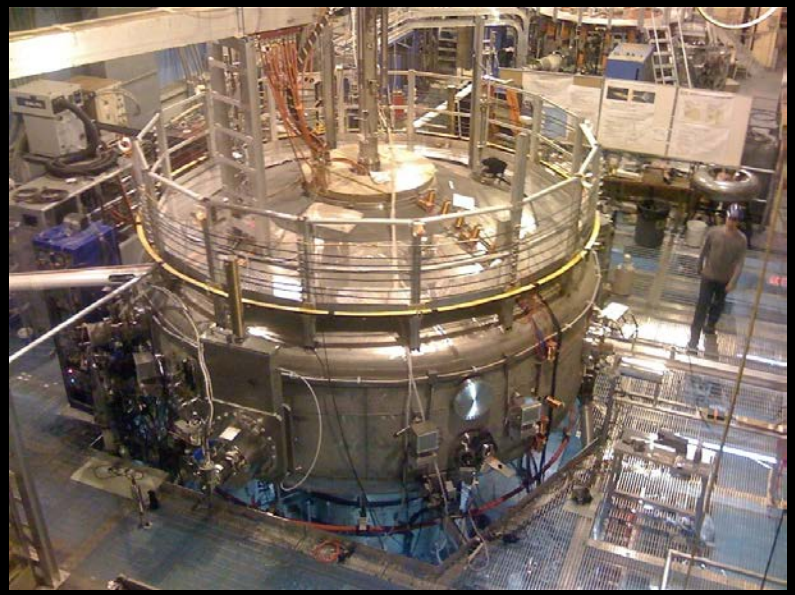

LDX:
High Beta Levitation & Turbulent Pinch

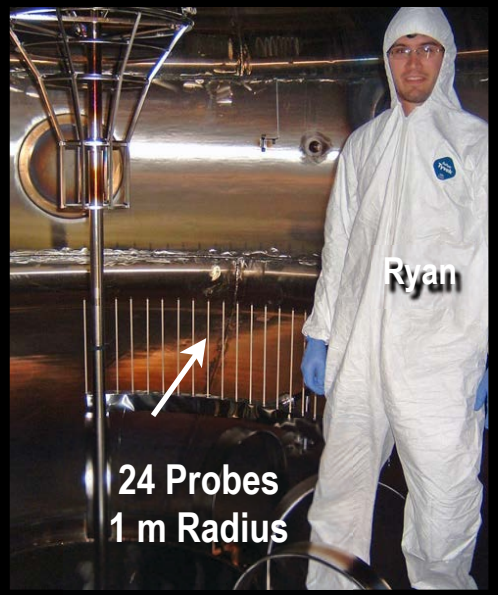

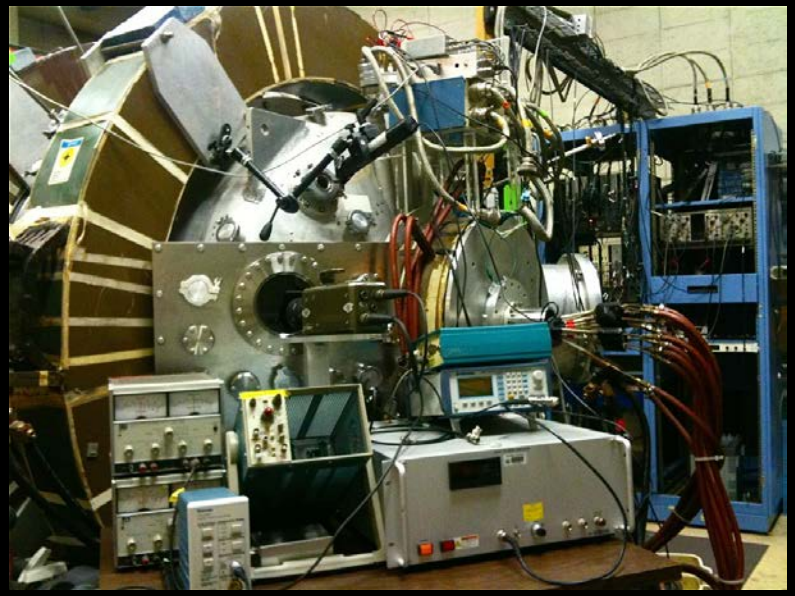

CTX:
Polar Imaging,
Current Injection.
Rotation

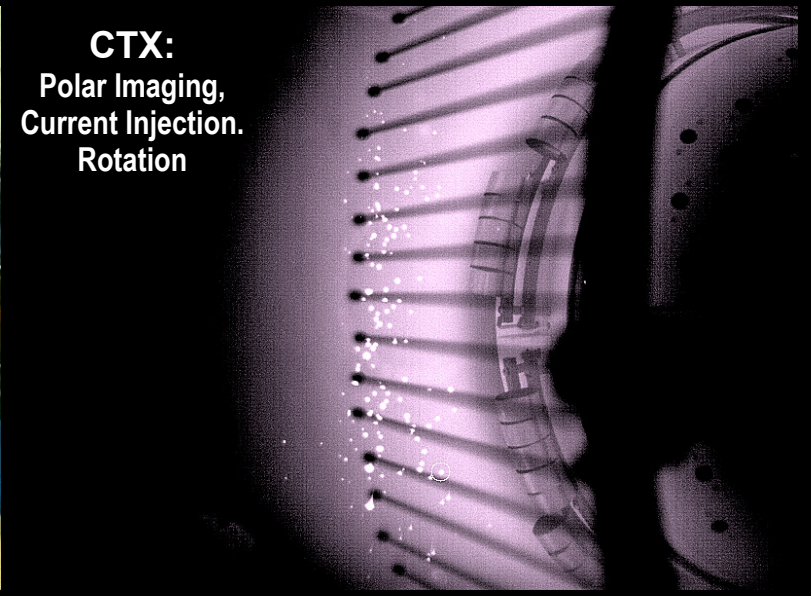

Flux-Tube Averaging Reveals Processes that Regulate Interchange Motion

$$\int \frac{ds}{B} \nabla_\perp \cdot \mathbf{J}_\perp = \begin{cases} 0 & \text{Closed, insulated, field lines} \\ 2(J_{||}/B)_{poles} & \text{Ionospheric current} \\ \sum_j I_j \, \delta(\psi - \psi_j)\delta(\phi - \phi_j) & \text{External circuits} \end{cases}$$

Steady MHD Convection in Space

$$\hat{\mathbf{b}} \cdot \nabla \Phi = 0$$

Dynamic Drift-like Motion in Lab

$$\mathbf{J}_\perp = \frac{\hat{\mathbf{b}} \times \nabla P}{B} \text{ (space)}$$

$$\frac{2J_{||}}{B_{pole}} = \nabla_\perp P \cdot \hat{\mathbf{b}} \times \nabla_\perp \int \frac{ds}{B}$$

$$\nabla_\perp \cdot \Sigma_p \nabla_\perp \Phi \approx -J_{||}(\hat{\mathbf{b}} \cdot \hat{\mathbf{n}}) \text{ (poles)}$$

Ionospheric Conductivity

Ion Inertial Currents

$$\mathbf{J}_\perp = \frac{\hat{\mathbf{b}} \times \nabla P}{B} - \frac{nM_i}{B^2} \nabla_\perp \frac{d\Phi}{dt}$$

$$\int \frac{ds}{B} \nabla_\perp \cdot \mathbf{J}_\perp = 0$$

$$\nabla_\perp \cdot \bar{\Sigma} \cdot \nabla_\perp \frac{\partial \Phi}{\partial t} \approx -\nabla_\perp P \cdot \hat{\mathbf{b}} \times \nabla_\perp \int \frac{ds}{B}$$

Integrated Plasma Dielectric

Vasyliunas, "Mathematical Models of Magnetospheric Convection and Its Coupling to the Ionosphere," in *Particles and Fields in the Magnetosphere*, edited by B.M. McCormac (D. Reidel, Norwell, MA, 1970), pp. 60–71.

Planetary Magnetospheres

$$U_{con} \cong \frac{c^2}{8\pi \Sigma_p} \cdot \frac{\ell_{\parallel}}{L_{ps}} \cdot \ell n \left(\frac{p_{tot}^{(24)}}{p_{tot}^{(12)}} \right)$$

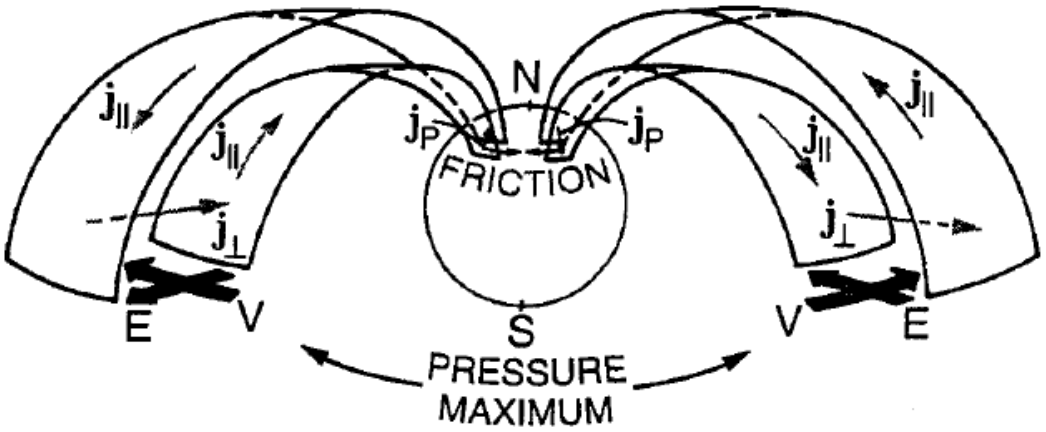

Figure 3. Dynamo forces, auroral current system, and resulting convection under frictional control by the ionosphere, after Boström (1964).

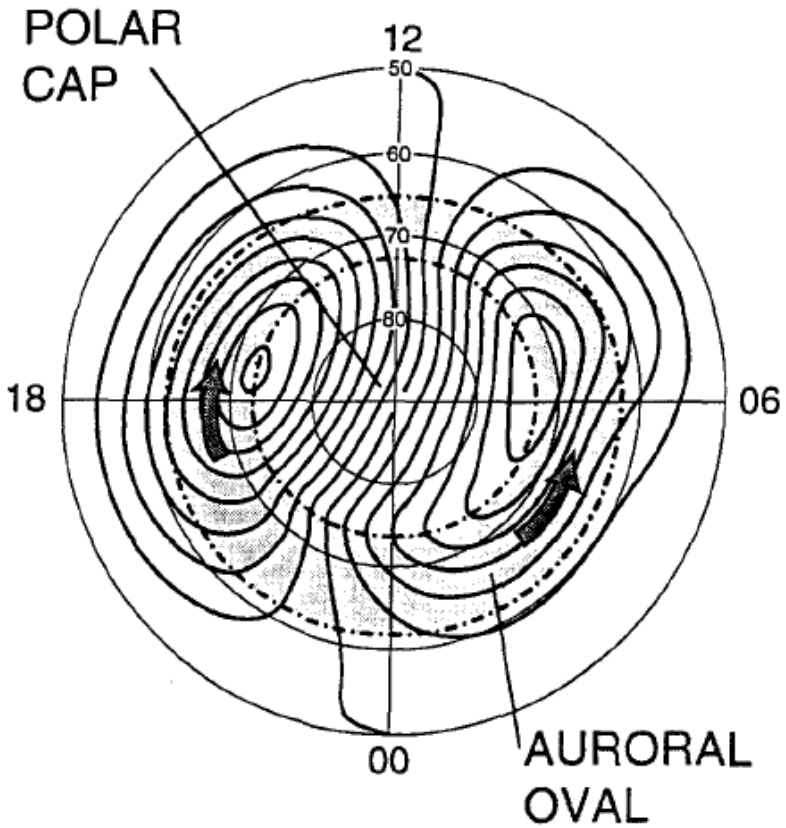

Figure 4. High-latitude plasma circulation system at times of an active magnetospheric dynamo (*e.g.* during substorms).

G. Haerendel, "Outstanding issues in understanding the dynamics of the inner plasma sheet and ring current during Storms and Substorms," *Advances in Space Research,* **25**, 2379 (2000).

Measured Ionospheric Currents

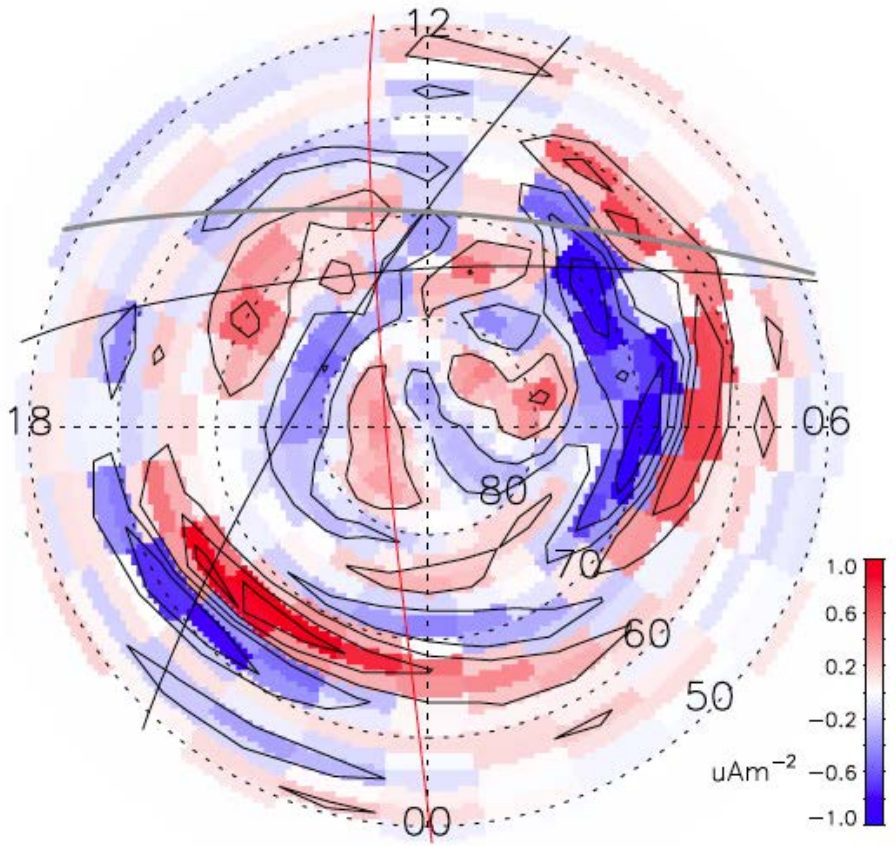

Fig. 6. Birkeland currents, $J_{\parallel}$ derived from the data in Fig. 4 according to Eq. (12) for 03:30–04:30 UT, 1 November, 2001. The DMSP and Oersted tracks are reproduced while the thicker, grey solid line from 06:00 to 18:00 MLT indicates the sunlight terminator boundary in the ionosphere.

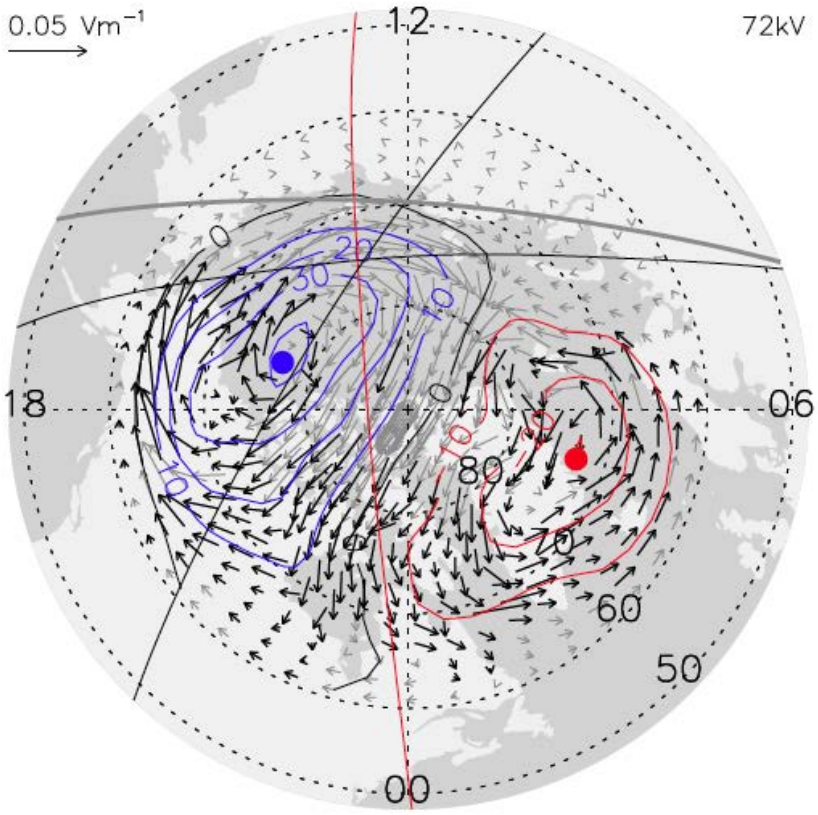

Fig. 7. Electric field vectors (rotated 90° counter clockwise) calculated from SuperDARN data averaged over 03:30–04:30 UT, 1 November, 2001. The electric potential contours, DMSP and Oersted tracks and the sunlight terminator are overlayed. The extremes in potential are located at the blue (-ve) and red (+ve) dots. The electric field vectors are bold at locations where radar returns were received.

Green, *et al.*, "Comparison of large-scale Birkeland currents determined from Iridium and SuperDARN data," *Annales Geophysicae* **24**, 941 (2006).

Measured Flute-Type Modes in CTX

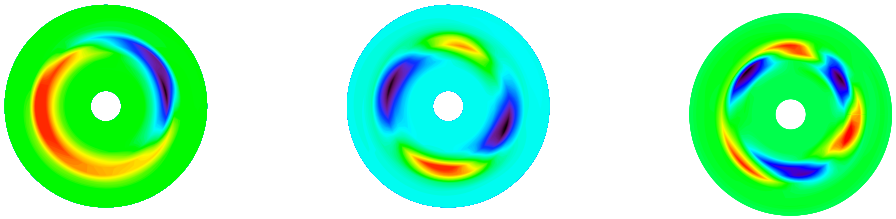

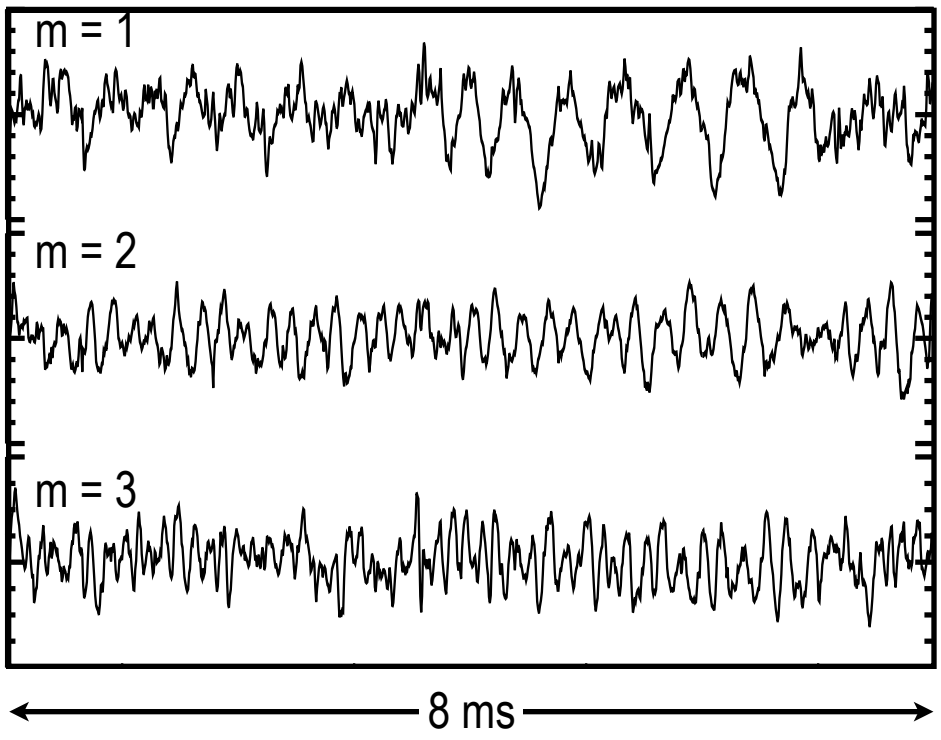

Convective Structures are Dynamic

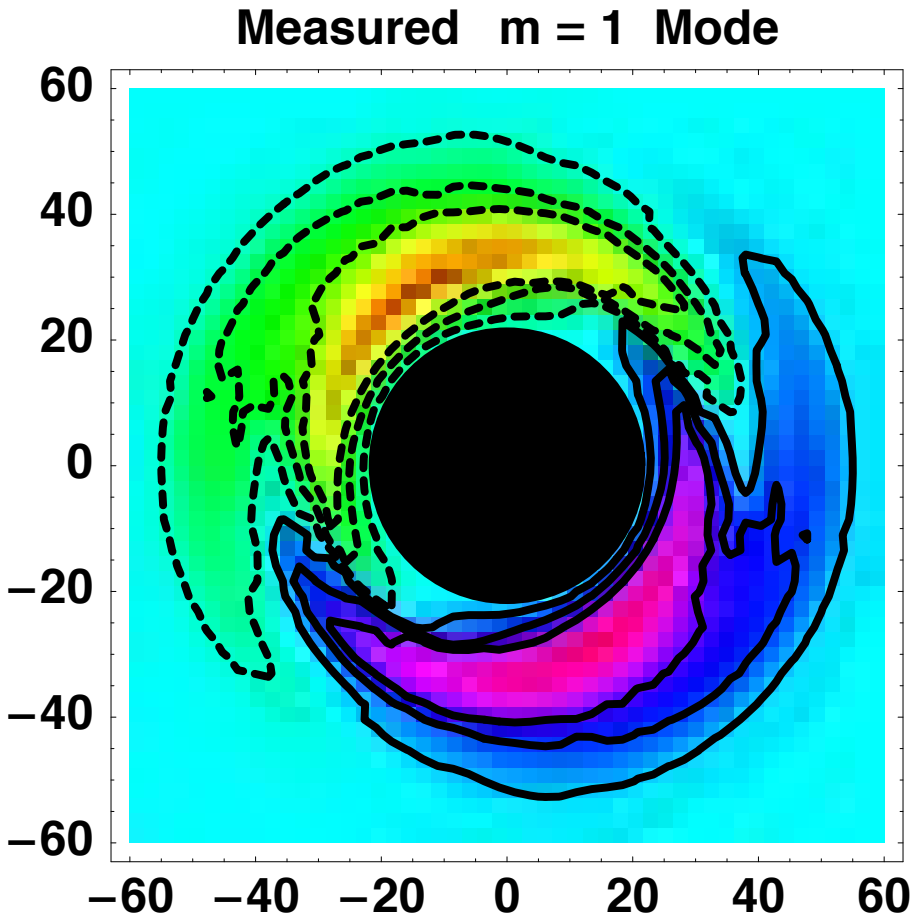

(ϕ ~ Stream function)

With $T_e >> T_i$ (CTX and LDX) modes (usually) propagate in electron drift direction

Fast MHD Interchange in an Axisymmetric Magnetic Dipole

$$\mathbf{B} = \nabla\phi \times \nabla\psi \qquad \mathbf{B}\cdot\nabla = 0$$

- Electrostatic, low β
- $V_\perp = E \times B$
- Adiabatic
- ➡ Flux-tube averaged
- 2D: (φ, ψ)
- *Missing*: Entropy and drift-interchange modes

$$N(\varphi,\,\psi,\,t) = \int \frac{ds}{B} n, \;\; \text{(Particle Number)}$$

$$P(\varphi,\,\psi,\,t)\,U(\psi) = \int \frac{ds}{B} P, \;\; \text{(Isotropic pressure)}$$

$$\frac{\partial U}{\partial \psi} = \int \frac{ds}{B}\,\nabla\varphi \cdot \frac{2}{B}\hat{b}\times\kappa = -2\langle\kappa_\psi\rangle U$$

$$\int \frac{ds}{B}\nabla_\perp\cdot\mathbf{J}_p = \frac{\partial U}{\partial\psi}\frac{\partial P}{\partial\varphi} \;\; \text{(diamagnetic)}$$

$$\int \frac{ds}{B}\nabla_\perp\cdot\mathbf{J}_i = -\frac{\partial}{\partial\psi}\left(N\,\Sigma_\psi\frac{\partial\dot{\Phi}}{\partial\psi}\right) - \frac{\partial}{\partial\varphi}\left(N\,\Sigma_\varphi\frac{\partial\dot{\Phi}}{\partial\varphi}\right)$$

$$\Sigma_\psi,\;\Sigma_\varphi = \frac{1}{N}\int\frac{ds}{B}\frac{nM_i}{B^2}|\nabla\psi|^2,\;\ldots, \;\; \text{(Polarization)}$$

Linearized dimensionless MHD dynamics Depends only upon ρ^* and profiles, h_n and h_g

- Equatorial radius, L_0
- Flux, $\psi_0 = B_0 L_0^2$ ($y \equiv \psi/\psi_0$)
- Gyroradius, $\rho^* = C_s / \omega_{ci} L_0 \ll 1$
- Potential, $M_i C_s^2/e$
- Pressure, $M_i C_s^2$
- Time, $1/(\omega_{ci}\, \rho^{*2})$

$$h_n' = \omega_n^* - \omega_d$$
$$h_g' = \omega_p^* - \gamma\omega_d$$

$$\frac{\partial \tilde{N}}{\partial t} + \frac{dh_n}{dy}\frac{\partial \tilde{\Phi}}{\partial \varphi} = 0$$

$$\frac{\partial \tilde{P}}{\partial t} + y^{4\gamma}\frac{dh_g}{dy}\frac{\partial \tilde{\Phi}}{\partial \varphi} = 0$$

$$\rho_*^2 \frac{\partial}{\partial t}\left[\frac{\partial}{\partial y}\left(h_n \Sigma_\psi \frac{\partial \tilde{\Phi}}{\partial y}\right) + h_n \Sigma_\varphi \frac{\partial^2 \tilde{\Phi}}{\partial \varphi^2}\right] + \frac{4}{y^5}\frac{\partial \tilde{P}}{\partial \varphi} = 0$$

$$\text{When } h_n' \sim h_g' \sim 0, \text{ then } (\tilde{N},\, \tilde{P},\, \tilde{\Phi}) \to 0$$

$$h_n(y) \equiv N(\psi)/N(\psi_0) \text{ and } h_g(y) \equiv P(\psi)U^\gamma / P(\psi_0)U(\psi_0)^\gamma$$

Local MHD Interchange Modes

$$\left\{\tilde{\Phi}(\psi,\varphi,t),\tilde{P},\tilde{N}\right\}=\sum_m\left\{\Phi_m(\psi),P_m(\psi),N_m(\psi)\right\}e^{-j(\omega_m t-m\varphi)}$$

$$\omega\tilde{N}-mh_n'\tilde{\Phi}=0$$

$$\omega\tilde{P}-mh_g'\tilde{\Phi}=0$$

$$\rho_*^2\omega\, m_\perp^2\Sigma_\varphi\tilde{\Phi}+4m\tilde{P}=0$$

m = 1, γ = 0.31/ρ*

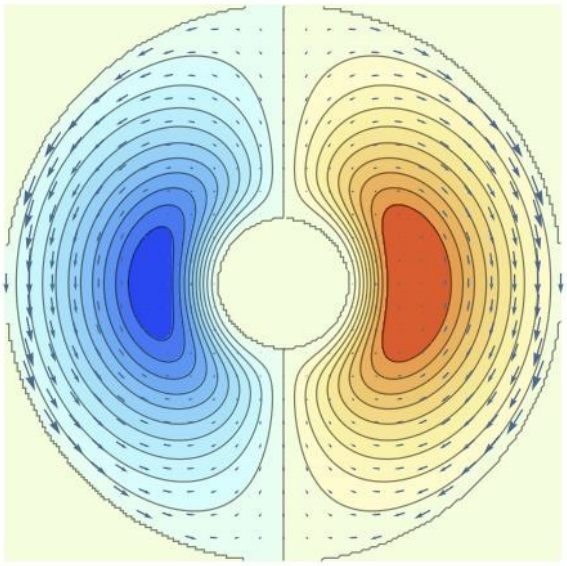

m = 4, γ = 0.34/ρ*

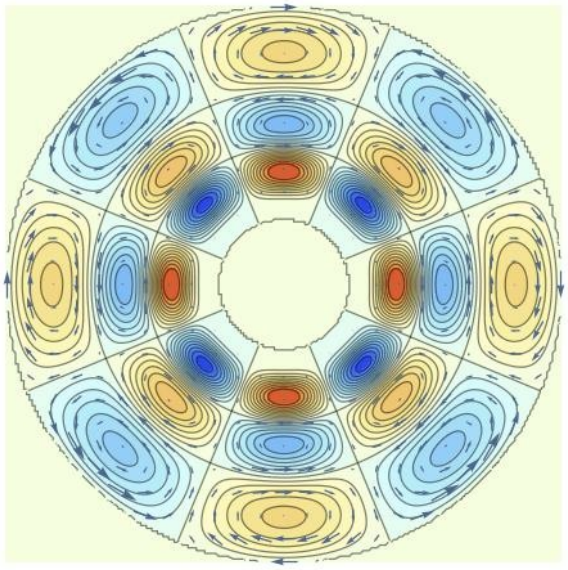

Example Eigenmodes: Unstable MHD Convection

$$\omega=\pm\frac{2.5}{\rho^*}\,\frac{m}{m_\perp}\sqrt{-h_g'}\;\begin{cases}\omega_p^*>\gamma\omega_d, & \text{unstable}\\ \omega_p^*<\gamma\omega_d, & \text{stable}\end{cases}$$

$$\omega\propto\omega_{ci}\rho^*$$

Adding magnetic drift physics uncovers Entropy and Drift-Interchange Modes

- Near marginal stability, diamagnetic flows and magnetic drifts modify interchange dynamics in a significant and fundamental way…
- Flute-type entropy modes become unstable unless $\eta \sim 2/3$
- Density and pressure drift perturbations exist even for stationary profiles (*i.e.* $h'_n \sim h'_g \sim 0$)
- Entropy and drift-interchange instabilities propagate toroidally
- See…
  - Kesner, *Phys Plasmas*, **7**, 3887 (2000)
  - Ricci, Rogers, Dorland, and Barnes, *Phys Plasmas* **13**, 062102 (2006)
  - Kobayashi, Rogers, and Dorland, *Phys Rev Lett,* **105**, 235004 (2010)

Entropy & Drift-Interchange Modes

(For CTX and LDX with $T_e >> T_i$)

ω_{de} flow

$$\frac{\partial \tilde{N}}{\partial t} + \frac{dh_n}{dy}\frac{\partial \tilde{\Phi}}{\partial \varphi} + \frac{4}{y^5}\frac{\partial \tilde{P}_e}{\partial \varphi} = 0$$

Collisionless heat flux due to Electron magnetic drift

$$\frac{\partial \tilde{P}_e}{\partial t} + y^{4\gamma}\frac{dh_g}{dy}\frac{\partial \tilde{\Phi}}{\partial \varphi} + \gamma\frac{4}{y^5}\left(\frac{y^{4\gamma}h_g}{h_n}\right)\left[2\frac{\partial \tilde{P}_e}{\partial \varphi} - \left(\frac{y^{4\gamma}h_g}{h_n}\right)\frac{\partial \tilde{N}}{\partial \varphi}\right] = 0$$

$$\rho_*^2\left(\frac{\partial}{\partial t} + \nu_i\right)\left[\frac{\partial}{\partial y}\left(h_n\Sigma_\psi\frac{\partial \tilde{\Phi}}{\partial y}\right) + h_n\Sigma_\varphi\frac{\partial^2 \tilde{\Phi}}{\partial \varphi^2}\right] + \frac{4}{y^5}\frac{\partial \tilde{P}_e}{\partial \varphi} = 0$$

ion-neutral damping

Local Entropy Drift-Interchange Modes

$$\omega\tilde{N} - mh_n'\tilde{\Phi} - 4m\tilde{P}_e = 0$$

$$\omega\tilde{P}_e - mh_g'\tilde{\Phi} - 4\gamma m(2\tilde{P}_e - \tilde{N}) = 0$$

$$\rho_*^2(\omega + i\nu_i)m_\perp^2\Sigma_\varphi\tilde{\Phi} + 4m\tilde{P}_e = 0$$

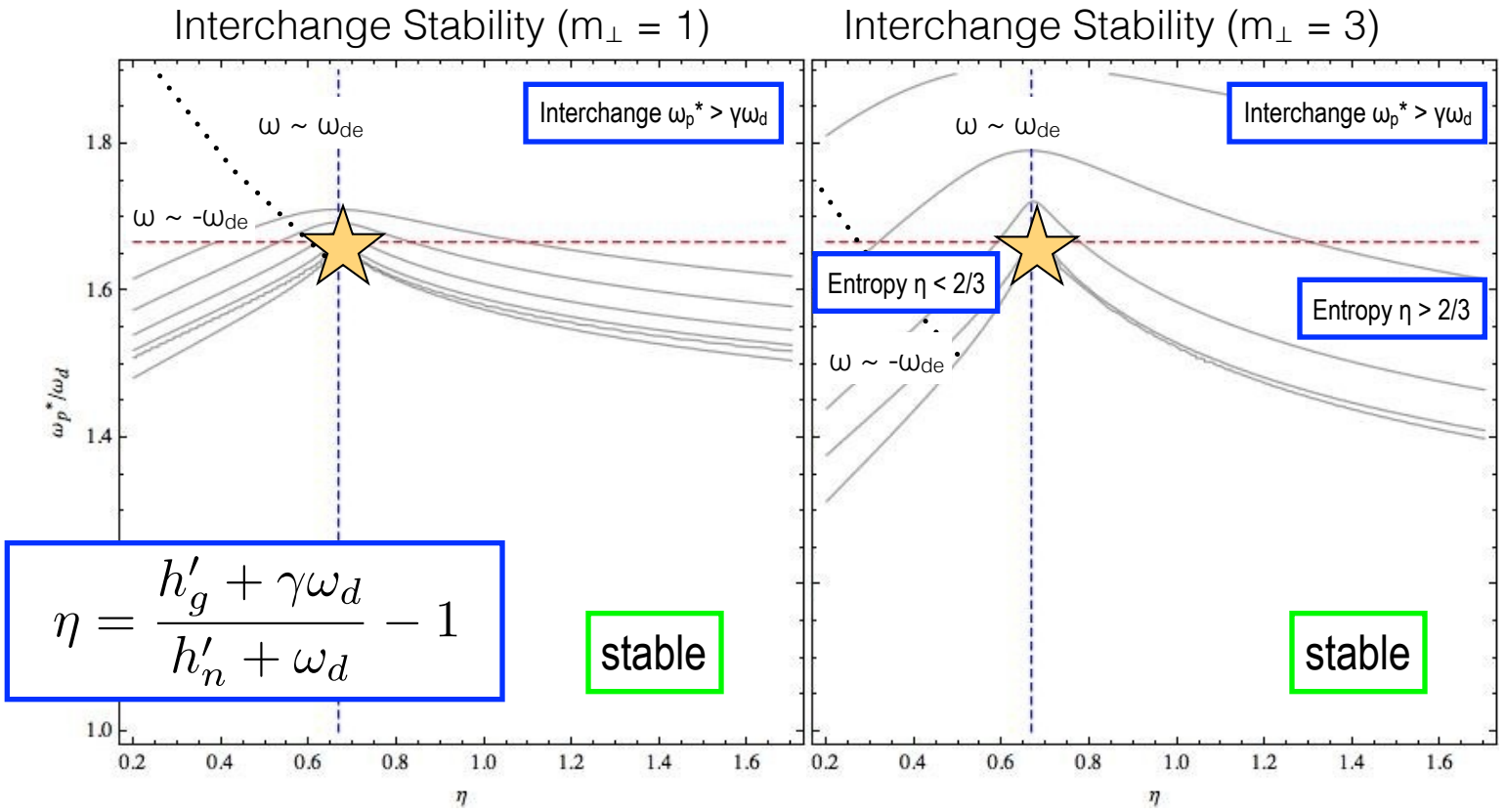

$$\eta = \frac{h_g' + \gamma\omega_d}{h_n' + \omega_d} - 1$$

m = 1 with ρ* = 1/25

★ "stationary"

Stationary Drift Waves in a Dipole with Warm Electrons

When $h_n' \sim h_g' \sim 0$, then two stable drift waves and a damped convective cell.

$$\omega_m = i\nu_i \qquad \text{with } \tilde{N} \sim \tilde{P}_e \sim 0$$

$$\omega_m = m\omega_d \left(\gamma + \sqrt{\gamma(\gamma-1)}\right) \qquad \text{“fast” drift wave}$$

$$\omega_m = m\omega_d \left(\gamma - \sqrt{\gamma(\gamma-1)}\right) \qquad \text{“slow” drift wave}$$

“Slow” and “fast” drift waves correspond to flux tubes with locally “cooler” or “warmer” electrons relative to average, N/P_e.

When $h_g' \sim 0$, then the “fast” drift mode becomes an unstable **entropy mode** when $h_n' > 0.54 m_\perp^2 \rho_*^2$ ($i.e.\ \eta > 2/3$) and the “slow” drift mode becomes unstable whenever $h_n' < -4.8 m_\perp^2 \rho_*^2$ ($i.e.\ \eta < 2/3$) .

Profiles in CTX and LDX

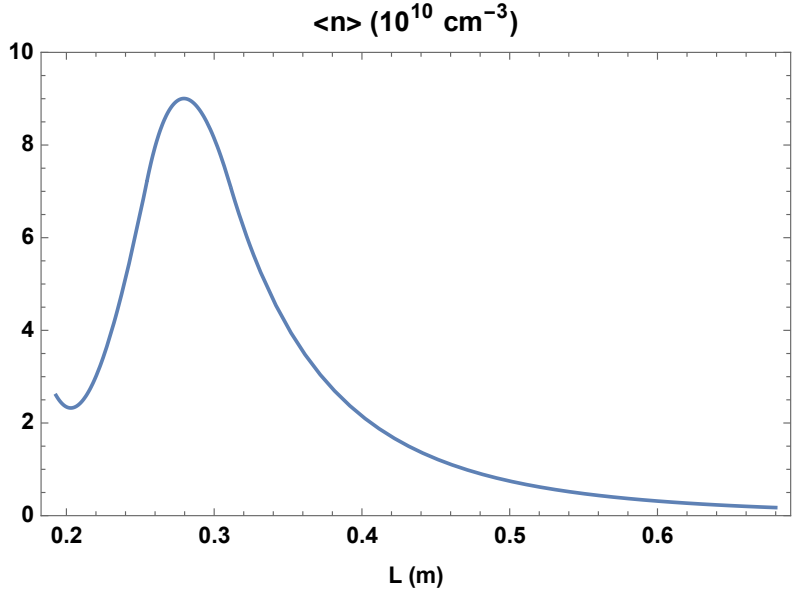

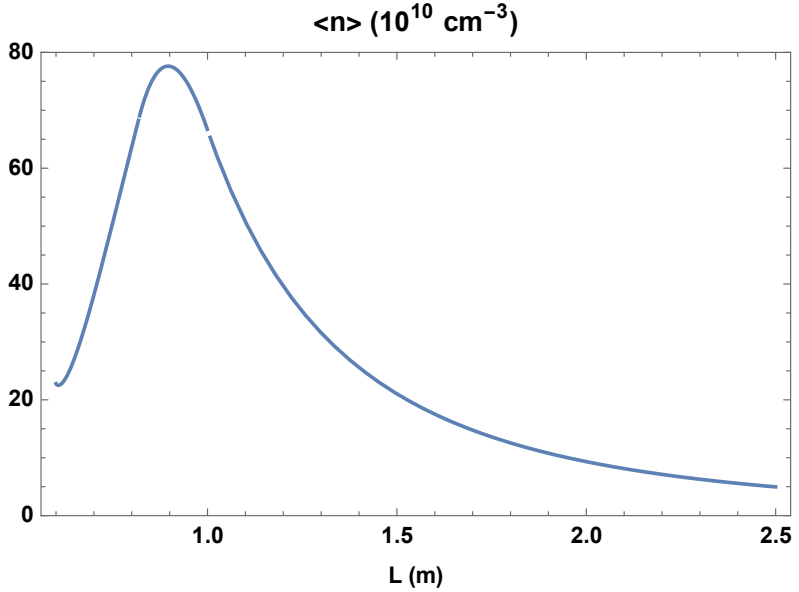

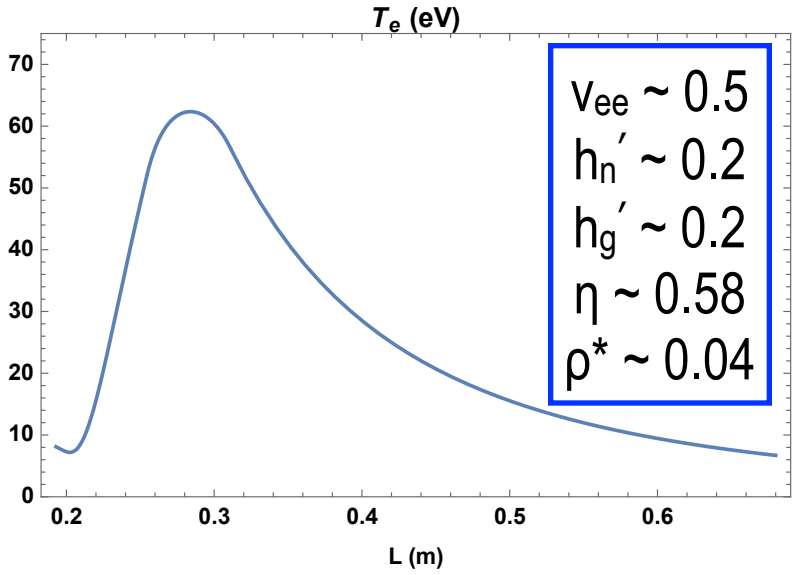

$\nu_{ee} \sim 0.5$
$h_n' \sim 0.2$
$h_g' \sim 0.2$
$\eta \sim 0.58$
$\rho^* \sim 0.04$

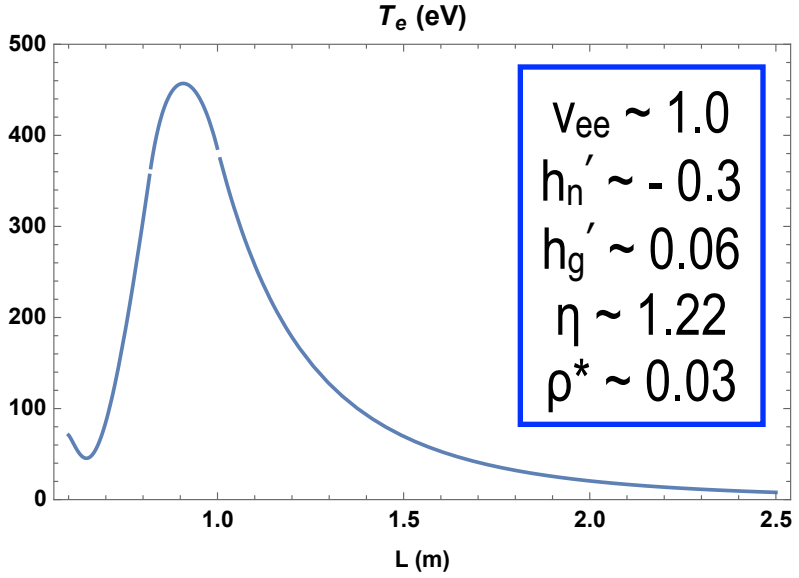

$\nu_{ee} \sim 1.0$
$h_n' \sim -0.3$
$h_g' \sim 0.06$
$\eta \sim 1.22$
$\rho^* \sim 0.03$

CTX and LDX have similar low-frequency flute-type dynamics

Example Drift-Interchange Eigenmodes

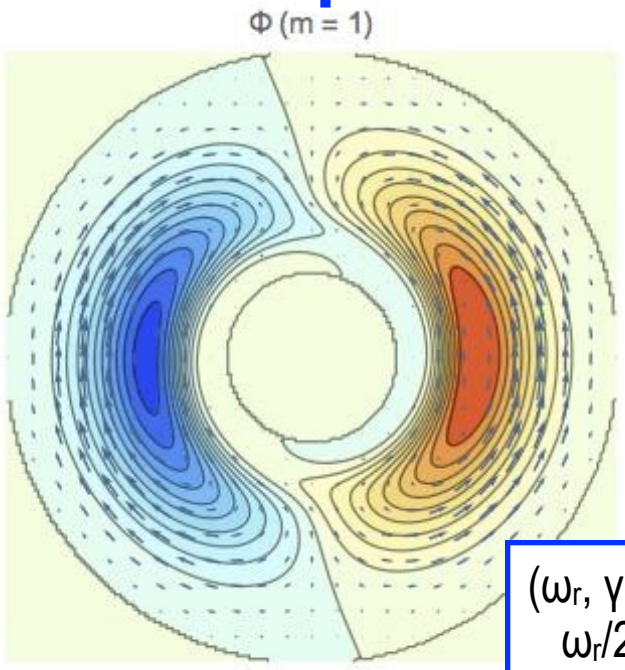

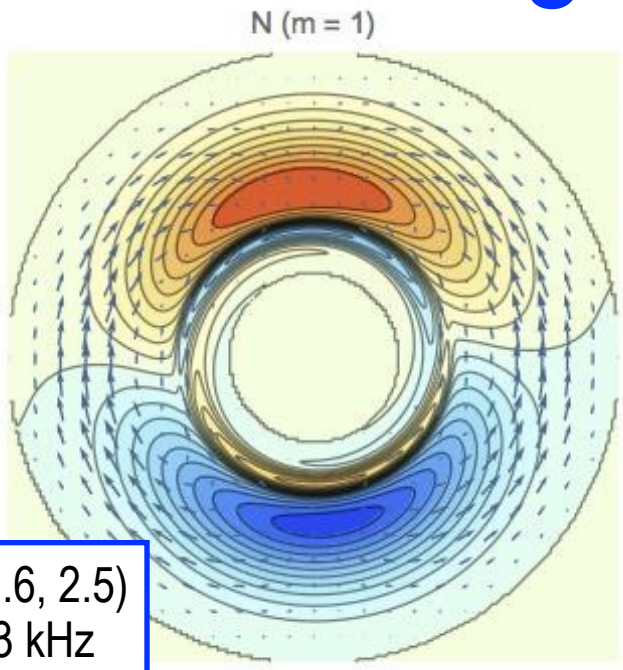

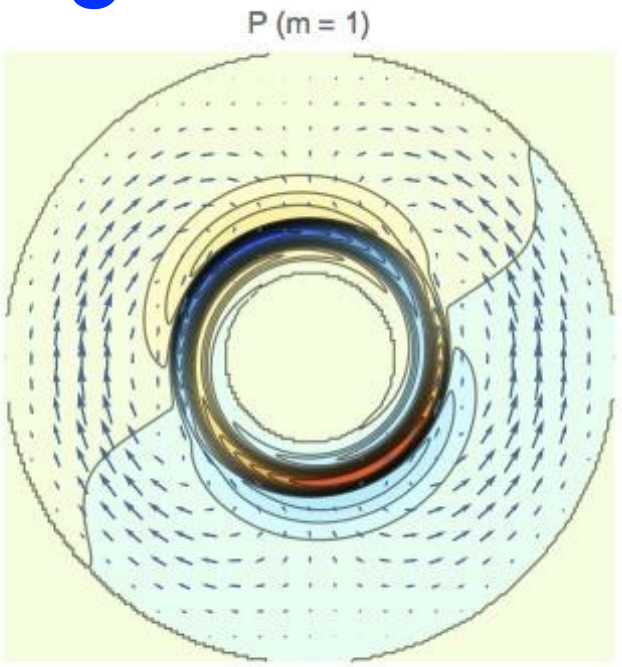

$(\omega_r, \gamma) = (1.6, 2.5)$
$\omega_r/2\pi = 3$ kHz

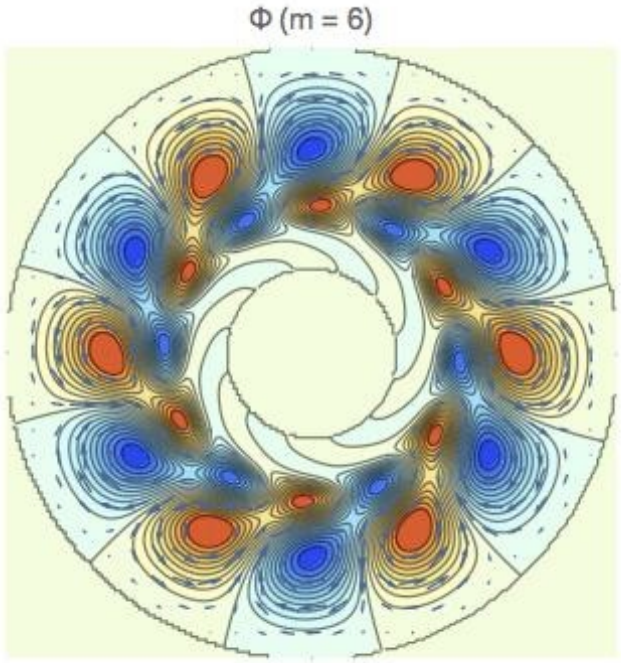

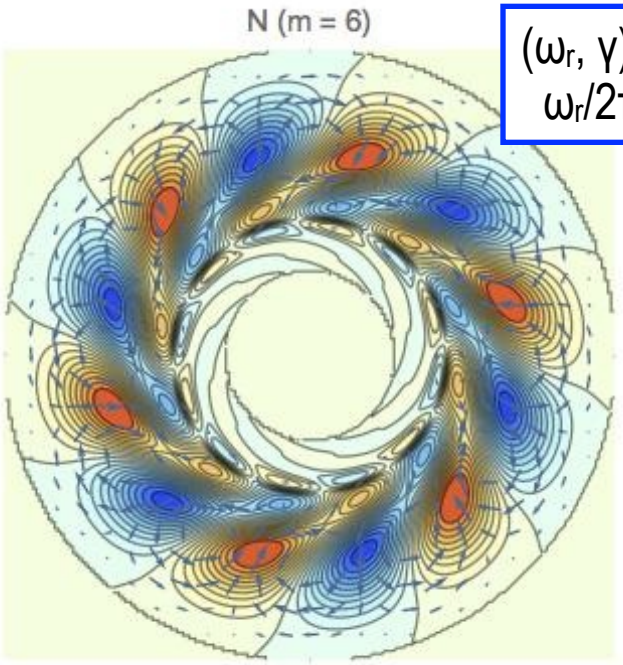

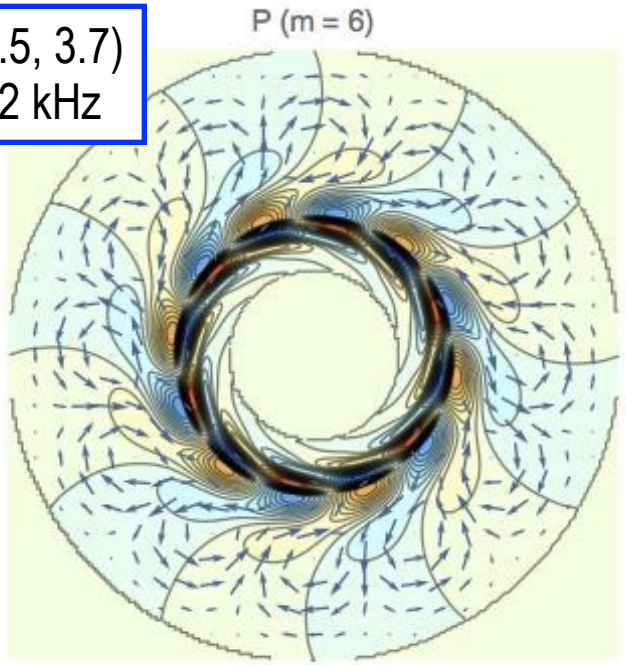

$(\omega_r, \gamma) = (6.5, 3.7)$
$\omega_r/2\pi = 12$ kHz

Example Entropy Mode Eigenmodes

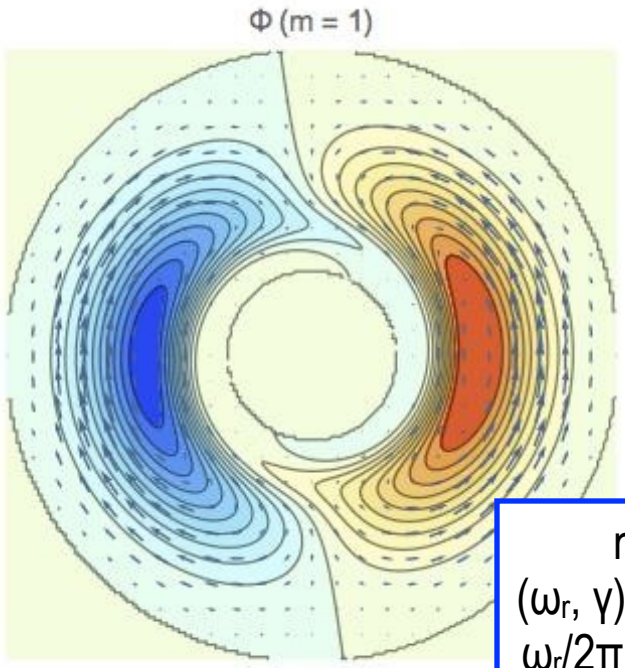

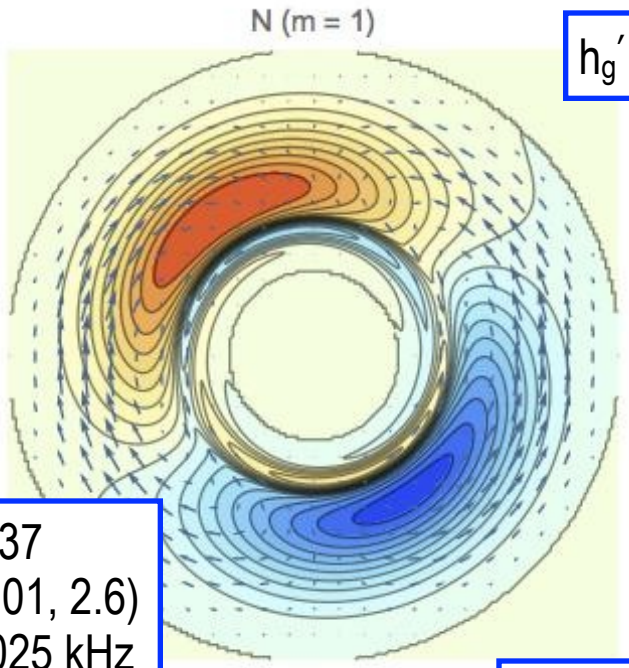

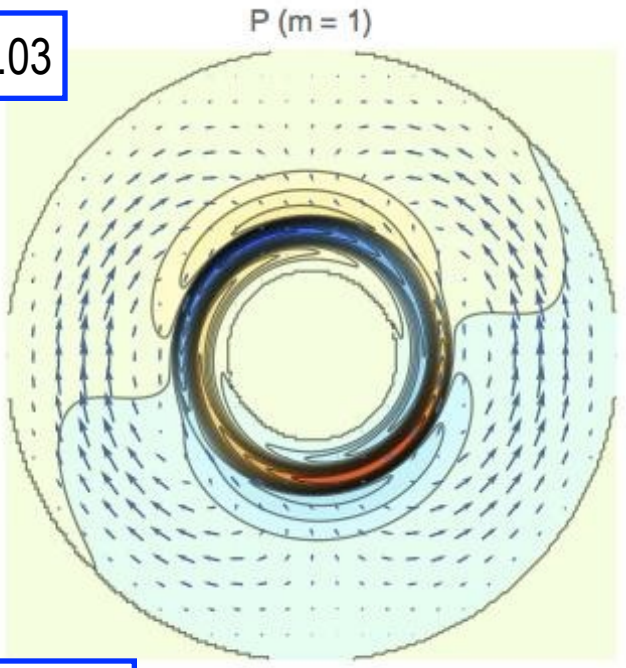

$h_g' = -0.03$

$\eta \sim 0.37$
$(\omega_r, \gamma) = (0.01, 2.6)$
$\omega_r/2\pi = 0.025$ kHz

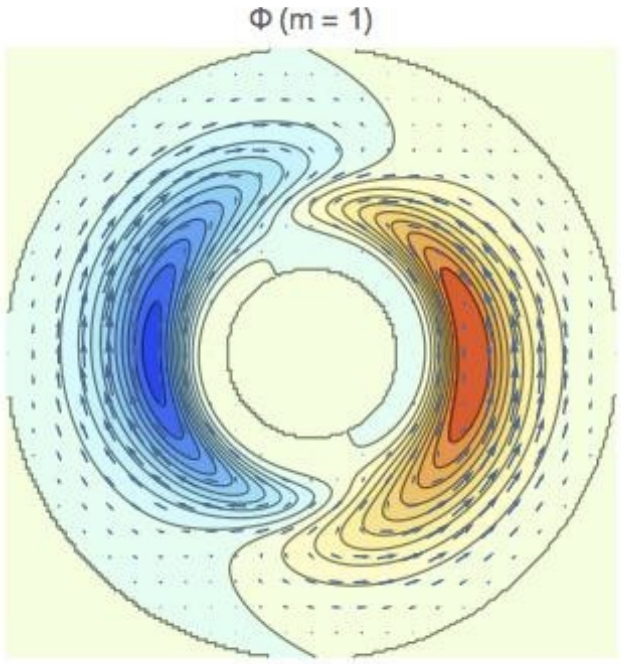

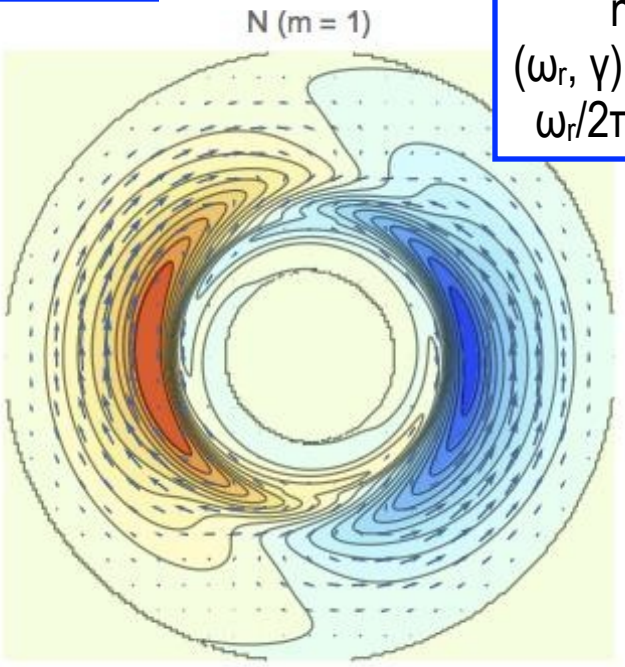

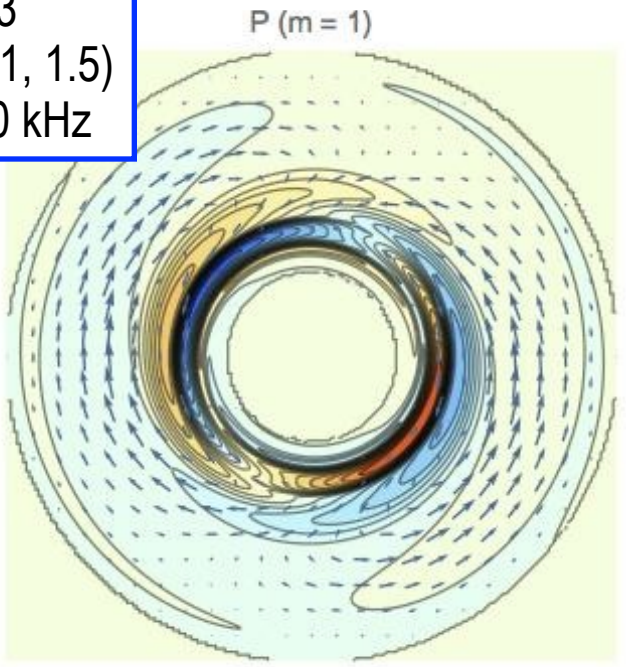

$\eta \sim 1.3$
$(\omega_r, \gamma) = (5.1, 1.5)$
$\omega_r/2\pi = 10$ kHz

PRL 105, 235004 (2010) PHYSICAL REVIEW LETTERS 3 DECEMBER 2010

Particle Pinch in Gyrokinetic Simulations of Closed Field-Line Systems

Sumire Kobayashi* and Barrett N. Rogers†
Department of Physics and Astronomy, Dartmouth College, Hanover, New Hampshire 03755, USA

William Dorland‡
Department of Physics, University of Maryland, College Park, Maryland 20742, USA
(Received 6 October 2010; published 2 December 2010)

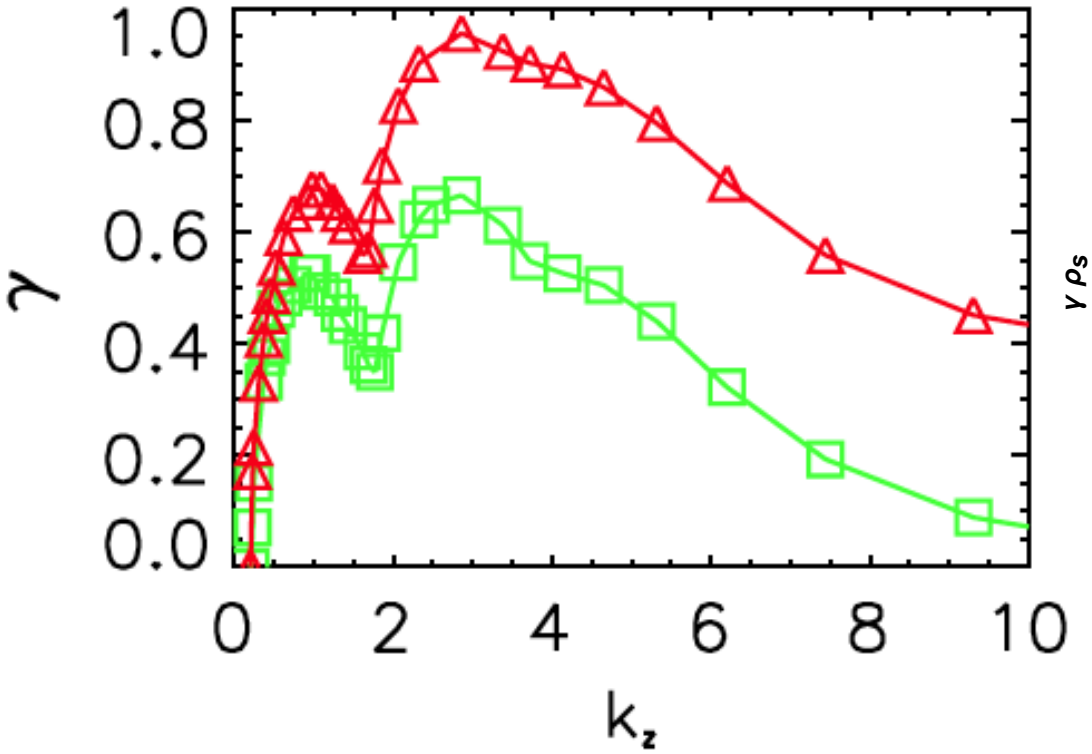

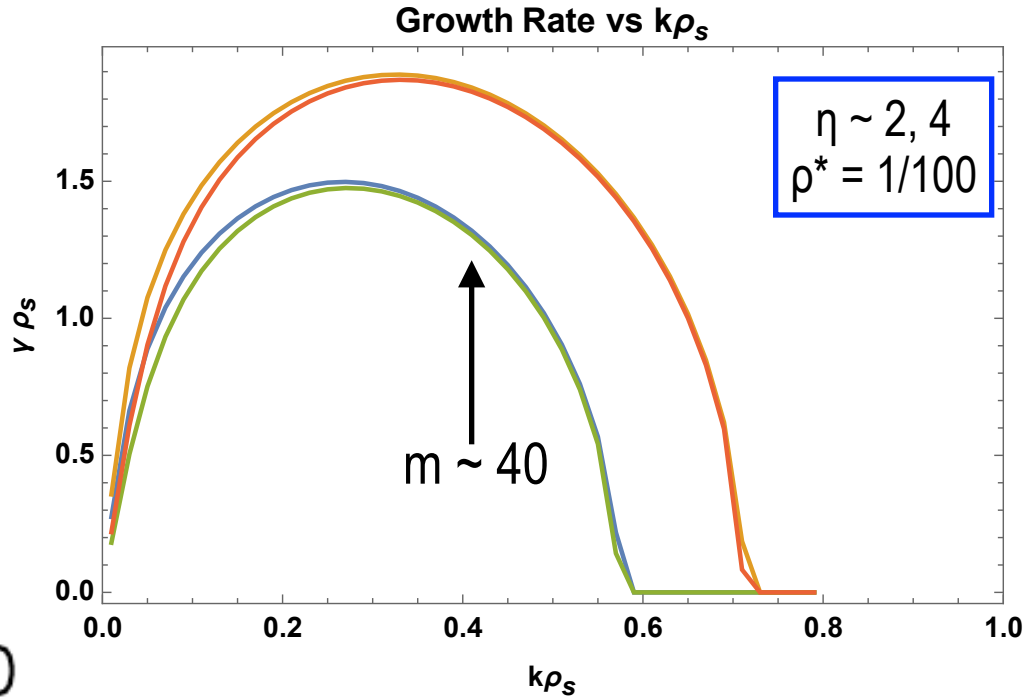

Peak growth rates for entropy mode have short wavelengths

Turbulent Intensity is Observed to Peak at Long Wavelengths (Inverse Mode-Mode Cascade)

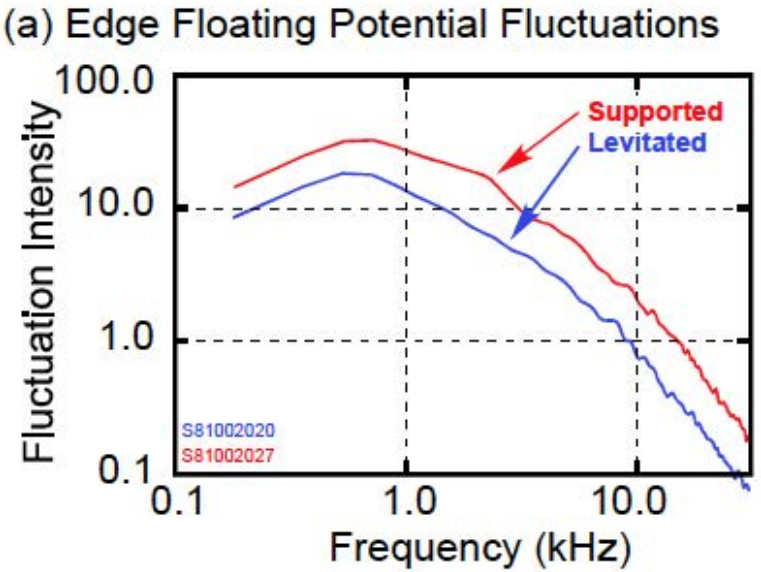

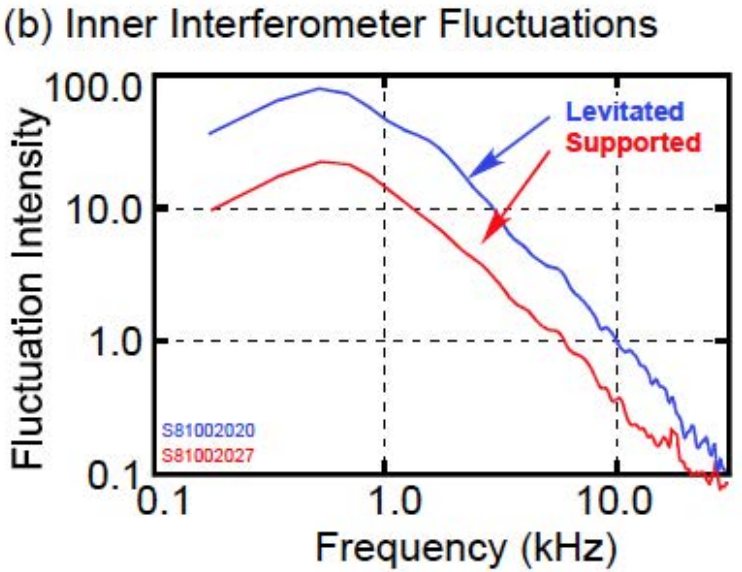

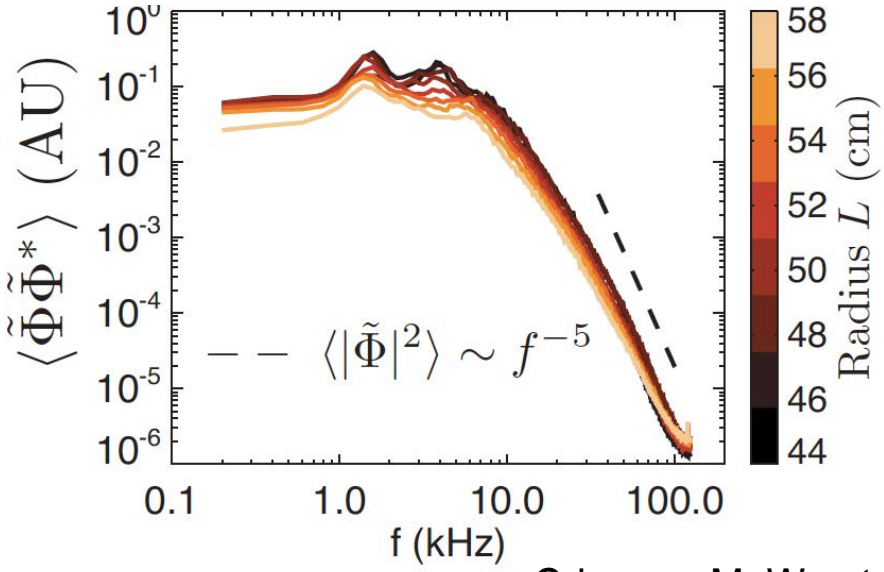

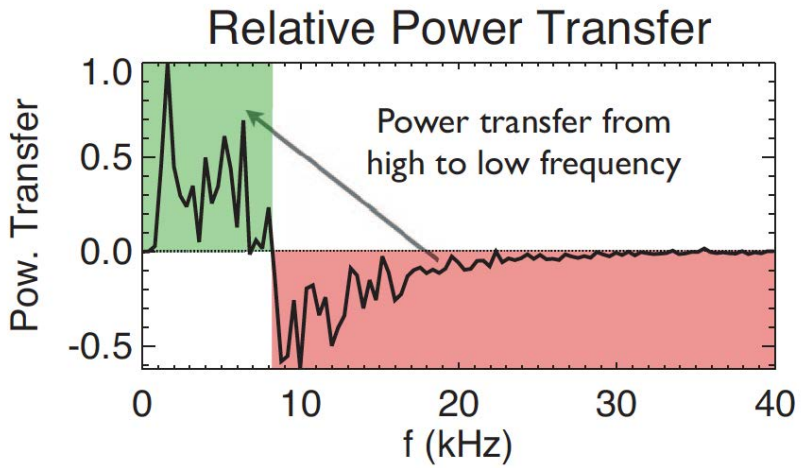

Grierson, M. Worstell, and M. Mauel, *Phys Plasmas* **16**, 055902 (2009).
Boxer, et al., *Nature Phys* **6**, 207 (2010).

Gyrofluid Quasilinear Theory

$$\frac{\partial \langle N \rangle}{\partial t} = -\frac{\partial}{\partial y} \sum_m \Re\{im\tilde{N}_m^* \tilde{\Phi}_m\}$$

$$\frac{\partial \langle G \rangle}{\partial t} = -\frac{\partial}{\partial y} \sum_m \Re\{im\tilde{G}_m^* \tilde{\Phi}_m\}$$

$$G \equiv PU^\gamma$$

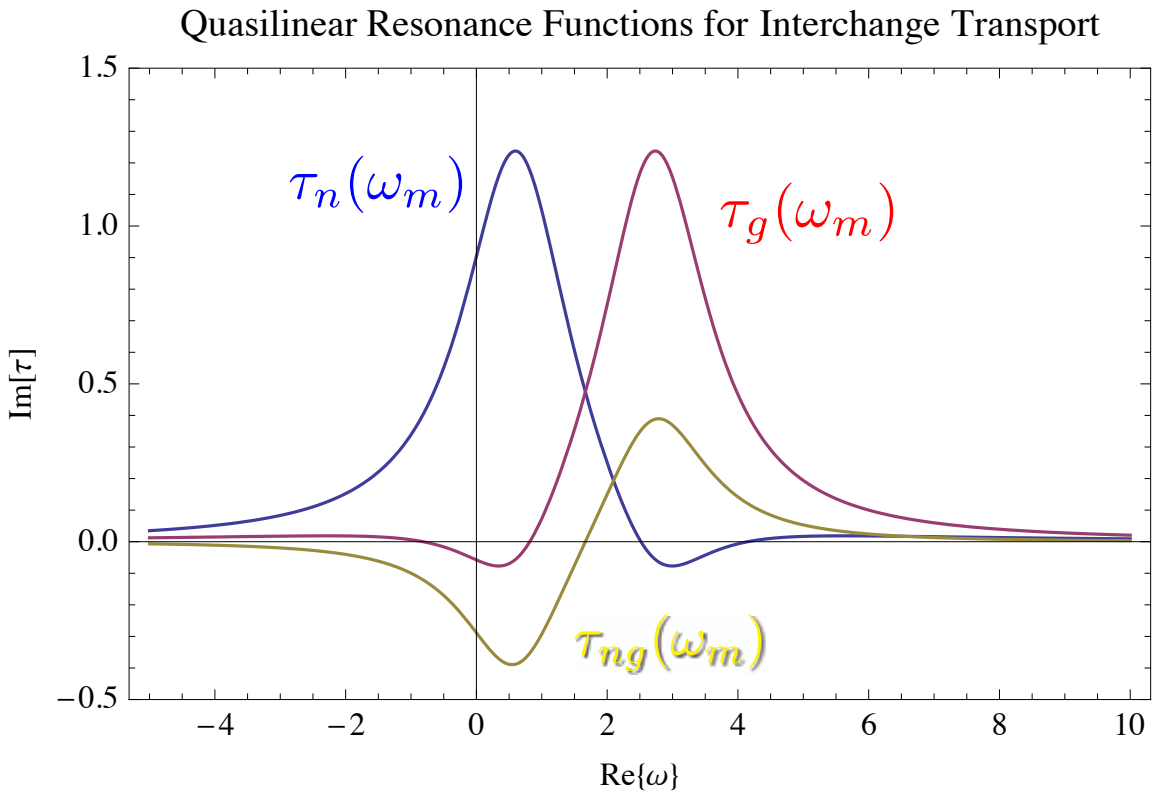

Figure 2: Plot of the quaslinear resonance functions in Eqs. 28 and 29, $\Im\{\tau(\omega_m)\}$, for weakly growing interchange modes as a function of the real mode frequency, ω/ω_d. The quasilinear diffusion coefficients are the summation, over all modes, of the product of the mode intensity and the resonance functions. The blue curve is τ_n; the red curve is τ_g; and the gold curve is the cross-diffusion, τ_{ng}.

$$\tilde{N}_m = m\tilde{\Phi}_m \left(\tau_n(\omega_m) \frac{\partial \langle N \rangle}{\partial y} + \tau_{ng}(\omega_m) \frac{\partial \langle G \rangle}{\partial y} \right)$$

$$\tilde{G}_m = m\tilde{\Phi}_m \left(\tau_g(\omega_m) \frac{\partial \langle G \rangle}{\partial y} - \gamma\tau_{ng}(\omega_m) \frac{\partial \langle N \rangle}{\partial y} \right)$$

Quasilinear Theory Description of Particle and Pressure Pinches includes Cross-Gradient Flux

Using these linear forms for the perturbed density and pressure, the quasilinear transport equations are

$$\frac{\partial\langle N\rangle}{\partial t} = \frac{\partial}{\partial y}\sum_m m^2|\Phi_m|^2\left(\Im\{\tau_n(\omega_m)\}\frac{\partial\langle N\rangle}{\partial y} + \Im\{\tau_{ng}(\omega_m)\}\frac{\partial\langle G\rangle}{\partial y}\right) \quad (28)$$

$$\frac{\partial\langle G\rangle}{\partial t} = \frac{\partial}{\partial y}\sum_m m^2|\Phi_m|^2\left(\Im\{\tau_g(\omega_m)\}\frac{\partial\langle G\rangle}{\partial y} - \Im\{\tau_{ng}(\omega_m)\}\frac{\partial\langle N\rangle}{\partial y}\right) . \quad (29)$$

Interchange transport fluxes have cross-terms that depend upon the frequency spectrum of the interchange turbulence. Peaked or hollow entropy density, $\partial\langle G\rangle/\partial y \neq 0$, can drive diffusion in flux-tube particle number, and peaked or hallow density, $\partial\langle N\rangle/\partial y \neq 0$, can drive diffusion in plasma pressure. The magnitude of the quasilinear fluxes depend upon the frequency spectrum. For a uniform turbulence spectrum, extending beyond a few times ω_d, the cross-diffusion fluxes vanish.

$$G \equiv PU^\gamma$$

Summary and Applications

- Global flux-tube averaged gryo-fluid description of flute-type instabilities describes drift-interchange and entropy modes
- Long wavelength eigenmodes and real frequencies resemble observations in CTX and LDX
- Quasilinear theory describes up-gradient turbulent pinches
- Linear theory can model local current-injection feedback (Roberts, *Invited Talk*, Wed morning)
- Need to include gyro-kinetic drift-resonances, like Maslovsky, Levitt, and Mauel, *Phys Rev Lett* **90**, 185001 (2003) and Beer and Hammett, *Phys Plasmas* **3**, 4018 (1996)
- Mode-mode and 2D interchange cascade may explain the discrepancy between observations dominated with low-*m* eigenmodes and linear high-*m* eigenmodes with large growth rates.
- Flux-tube averaging makes possible “whole-plasma” nonlinear turbulence simulations.